JMEPEG (2011) 20:1671–1677
DOI: 10.1007/s11665-011-9833-3

1059-9495/$19.00

The Influence of Retained Austenite on Residual Stresses in Laser Remelted Cast Iron

Roman Šturm and Janez Grum

(Submitted June 11, 2010; in revised form December 17, 2010)

The presence and amount of residual stresses is very important in dynamically loaded automotive machine parts. In this investigation, the residual stresses after laser surface remelting were measured as a function of the modified layer depth on flat specimens from nodular cast iron. The results of the measured residual stresses confirm that the stresses strongly depend on the presence and quantity of the microstructure constituents in the surface remelted layer. Residual stresses have a characteristic profile in the modified surface layer. In the surface remelted layer, tensile residual stresses were found in a range between +70 and +200 MPa. The change from tensile into compressive residual stresses takes place in the lower part of the remelted layer. Maximum compressive residual stress values were found in the middle of the hardened layer in a range between −25 and −80 MPa.

Keywords constituents, laser surface remelting, nodular cast iron, residual stresses, retained austenite

1. Introduction

Cast irons are widely used in engineering practice because of their low price, good cast-ability, and good machine-ability, all desirable features for automotive application. Parts for automobile engines made from cast irons, like engine cam and follower, cylinder bore, valve seats, can be given a considerably better wear resistance by modifying the surface of the most exposed parts by laser heat treatment (Ref 1-6).

Laser remelting is of commercial interest because of its ability to alter with accuracy the properties of localized surface regions without reprocessing the material as a whole. By choosing a suitable energy input, we can achieve rapid local heating up to the austenitic region or even the temperature of the surface layer melting which, after the cooling process is completed, enables us to obtain a modified layer of desired depth. Rapid heat transfer into the remaining part of the cold mass can quite easily achieve the required surface layer cooling rates (Ref 7, 8). Thus, the aim of surface remelting process is to ensure a fine-grained microstructure with uniform microhardness, which cannot be achieved by other procedures for surface hardening of pearlite-ferrite cast irons (Ref 9). The properties of the modified layer depend on the microstructure prior to heat treatment and on the amount of energy input transferred to the surface layer of the specimen (Ref 10, 11). This study discusses the different effects of the laser remelting process on the microstructural changes in the surface layer as well as residual stresses developed in the nodular cast iron 500-7. Optimal laser remelting conditions were chosen, while only the overlapping of the remelted traces was varied. To measure the residual stresses, the relaxation method was used. The method includes gradual electro-chemical removal of the surface modified layer. Simultaneously, the deformation of the specimen was measured by resistance strain gauges.

Roman Šturm and **Janez Grum,** Faculty of Mechanical Engineering, University of Ljubljana, Aškerčeva 6, 1000 Ljubljana, Slovenia. Contact e-mail: roman.sturm@fs.uni-lj.si.

2. Material and Laser Remelting Conditions

For experimental testing of the laser surface remelting procedure, nodular cast iron 500-7 (according to ISO standard) was used. Nodular cast iron has had a pearlite-ferrite matrix (31% of pearlite and 69% of ferrite) with 10.76 vol.% of graphite nodules. The average diameter of graphite nodules was 30 μm. The chemical composition of the investigated nodular cast iron was: C = 3.77%, Si = 2.26%, Ni = 0.03%, Cr = 0.04%, Cu = 0.33%, Mn = 0.13% in wt.%, and carbon equivalent was CE = 4.53. Laser light absorptivity of the specimen surface (Ref 12) was increased by treating the specimen surface in a Zn-phosphate bath for 10′ at 50 °C. The laser surface remelting tests were performed with a CO_2 laser, with a maximum working power of 1.5 kW and a Gaussian distribution of energy in the beam. The tests were made with a laser power of 1.0 and 1.5 kW, the focal length of the focusing lens was 127 mm, and the defocusing distance of the beam was 22 and 34 mm. The laser beam travelling speed varied in the range from 18 to 21 mm/s. Laser parameters were changed to achieve energy input into the specimen material between E_i = 14.4 and 16.3 J/mm^2, which was preliminary found out as the optimal energy input range for our experiments.

Figure 1(a) shows the specimen dimensions (27 × 27 × 5 mm), and the mode of laser beam guiding over the specimen surface (zig-zag movement, where laser beam turns round outside the specimen). Figure 1(b) shows a schematic presentation of a cross section through the modified surface layer. To achieve a fully remelted surface area of the specimen, the kinematics of the laser beam were adapted so that a 0, 15, 30, or

50% overlapping of the width of the remelted traces was ensured. The overlapping in the remelted surface is expressed in percent with respect to the width of a single remelted trace.

3. Results

3.1 Microstructure Analysis

The microstructure of the surface modified layer consists of two characteristic microstructure layers: remelted and hardened layer. The average depth of the remelted layer was between 0.3 and 0.4 mm and the average depth of the whole modified layer was between 0.6 and 0.8 mm.

3.1.1 Remelted Layer. In the process of laser surface remelting, a very high solidification rate is achieved in the molten pool (Ref 7-13). Solidification effects lead to the occurrence of metastable phases with different compositions and a variety of microstructure scales (Ref 7, 14, 15). Figure 2(a) shows a characteristic microstructure of the remelted layer in nodular cast iron. The microstructure in the remelted layer has been confirmed by x-ray diffraction (XRD) phase analysis. The XRD analysis over the remelted surface is presented in Fig. 2(b). It was confirmed that remelted surface of nodular cast iron 500-7 consisted of retained austenite (Fe_γ), martensite ($Fe_{\alpha'}$), cementite (Fe_3C) and graphite (C) (Ref 16). Very rapid cooling rates in the thin surface remelted layer produces the following effects:

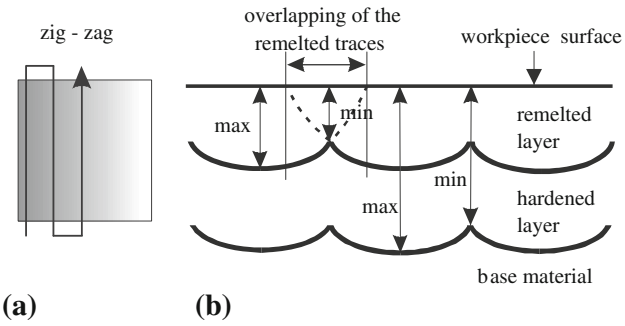

Fig. 1 Mode of laser beam guiding over the specimen surface (a) and cross section of laser surface modified layer (b)

- Incomplete dissolution of large graphite nodules;
- Redistribution of larger un-dissolved graphite nodules as a result of hydrodynamic and buoyancy forces in the molten pool;
- The hydrodynamic forces acting on the molten pool cause the pool to agitate and thus homogenize.

3.1.2 Hardened Layer. In the hardened layer, transformations occur in the solid state. During laser heating, the pearlite matrix transforms into a carbon-rich austenite, into which additional carbon diffuses from graphite nodules. During rapid self-cooling or self-quenching, the carbon-rich austenite transforms into martensite with some retained austenite.

During laser heating, the ferrite matrix transforms into an austenite with very low carbon concentration. But, at high temperatures carbon diffuses from graphite nodules into the austenite very fast. The diffusion path of carbon is a function of time and temperature. The measure for carbon solubility is the change in carbon concentration from the surface of a particular graphite nodule to the extreme point of diffusion path. Thus, during rapid cooling, hard ledeburite and/or martensite shells form around graphite nodules (Ref 17, 18), as it is shown in Fig. 3.

3.2 Microhardness Analysis

The results of microhardness measurements have confirmed the microstructure changes in the material. So, laser surface remelting is a successful method for hardening cast irons with non-homogeneous microstructure. The microhardness of the bulk pearlite material is between 200 and 250 $HV_{0.1}$. Hardness increases after laser surface remelting process. Microhardness of the remelted layer is between 650 and 950 $HV_{0.1}$. Microhardness of the martensite microstructure of the hardened layer is between 600 and 830 $HV_{0.1}$ (Fig. 4). We can note an effect of martensite tempering in the hardened layer when overlapping degree of the remelted traces is increased. This effect is to a large extent due to good heat conductivity of the ferrite part of the bulk matrix structure.

3.3 Residual Stress Analysis

The knowledge about the stress state in the surface remelted or heat affected layer is very often essential for parts which are subjected to dynamical loads. The residual stress variation in

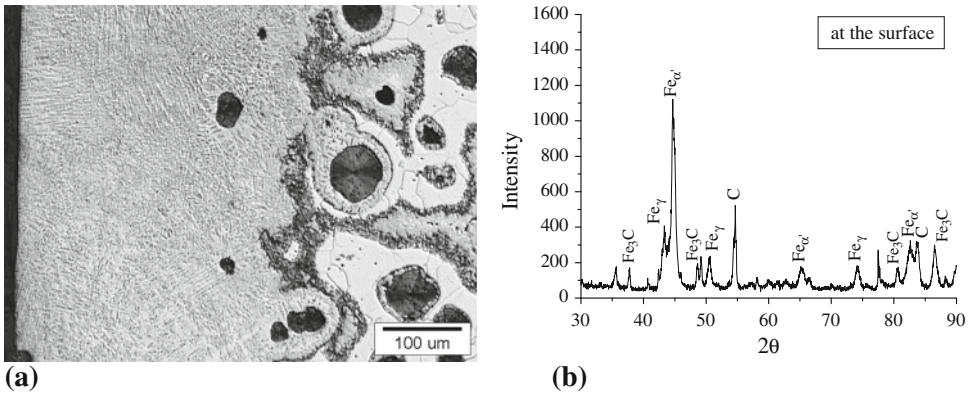

Fig. 2 Microstructure of the surface modified layer (a) and XRD analysis at the surface of the remelted layer (b): P = 1 kW, D_b = 3.3 mm, v_b = 21 mm/s, 30% overlapping of the remelted traces

the remelted layer can be described with concentration of retained austenite, martensite, and cementite in vol.%. Specific volumes of the microstructure constituents in relation to carbon concentration are given in Table 1 (Ref 19, 20). The reduction of volume of the material during phase transformation influences the origin of tensile residual stresses. Surface remelted layer with tensile internal stresses is, however, much more likely to develop cracks already during cooling of the remelted surface layer. These small cracks could later propagate and grow into a catastrophic failure of a specimen.

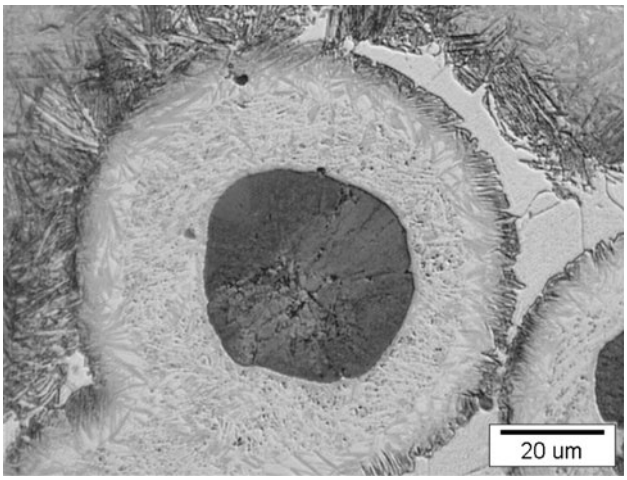

Fig. 3 Hard martensite/ledeburite shells around graphite nodules in hardened layer

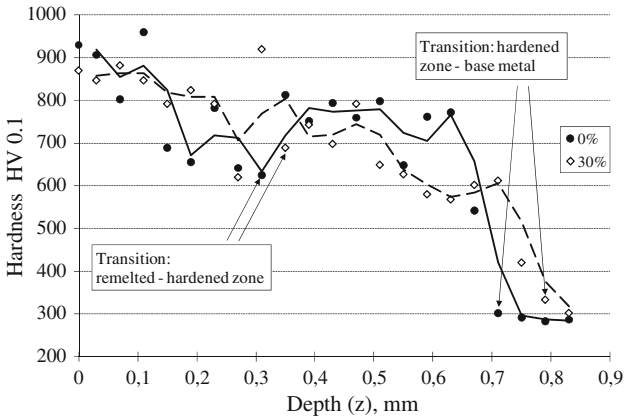

Fig. 4 Microhardness measurements cross the modified layer at different overlapping degrees of the remelted traces

Table 1 Specific volume of constituents

Constituent	Specific volume, cm^3/g
Austenite (Fe_γ)	$0.1212 + 0.0033 \cdot C$
Martensite ($Fe_{\alpha'}$)	$0.1271 + 0.0025 \cdot C$
Ferrite (Fe_α)	0.1271
Cementite (Fe_3C)	0.130

Carbon C in wt.%

The measurement system for measuring residual stresses by specimen deformation after electro-chemical dissolution is shown in Fig. 5. Residual stress measurement method is based on removing a thin layer of thickness Δh_i on one face of the specimen. Thin removed layer causes specimen deformation and a new stress distribution in the specimen. The principle of the presented method is to connect measured strains of the specimen with residual stresses present in the removed material. The result of the calculation is expected to represent the original residual stress distribution (Eq 1, 2) (Ref 21).

$$\sigma_h^R(j-1,0) = \frac{-\left(h_{j-1}-\Delta h_j\right)^2}{2\cdot\left(h_{j-1}+2\cdot\Delta h_j\right)\cdot\Delta h_j}\cdot B_j - \sum_{i=1}^{j-1}\left[-3\cdot\frac{h_{i-1}+\Delta h_i}{\left(h_{i-1}-\Delta h_i\right)\cdot\left(h_{i-1}+2\cdot\Delta h_i\right)}\cdot h_{j-1}+1\right]\cdot B_i \quad \text{(Eq 1)}$$

and

$$B_j = \frac{E}{1-\nu^2}\cdot\left(\Delta\varepsilon_{x,j}-\nu\cdot\Delta\varepsilon_{y,j}\right) \quad \text{(Eq 2)}$$

where the symbols signify: E (MPa) is the Young modulus, ν (/) is the Poisson ratio, h (mm) is the thickness of the specimen, Δh (mm) is the thickness of a layer, Δε (%) is the deformation of the specimen resulting from thin surface layer dissolution.

In Fig. 6, we can see the variation of residual stresses measured through thickness of the modified layer of nodular cast iron 500-7. Surface modified layer was obtained with laser energy input of E_i = 14.4 J/mm^2 (P = 1 kW, D_b = 3.3 mm, v_b = 21 mm/s) and at different degrees of overlapping. The first measurements of the residual stresses were done after removing initial 0.05 mm of material. From the results in Fig. 6 we can conclude the following:

- Residual stresses have very similar profiles through depth in all cases of different degrees of overlapping. The differences are in absolute values.
- In the surface remelted layer, tensile residual stresses were found in a range between +70 and +200 MPa.
- The change from tensile into compressive residual stresses takes place in the lower part of the remelted layer. Maximum compressive residual stress values were found in the middle of the hardened layer in a range between −25 and −80 MPa.

In Fig. 7, we can see the effect of laser pre-heating on residual stresses. Pre-heating was obtained by increasing laser beam power (P = 1.5 kW) and laser beam diameter on the specimen surface (D_b = 5.1 mm). Energy input E_i = 16.3 J/mm^2 was increased too. That results in lower cooling gradients and in tempering effects. So in the case of 50% overlapping of the remelted traces, microstructure with almost no residual stresses is produced.

The tensile residual stress variation in the remelted layer is very much dependent on the cooling conditions which can be described by the volume portion of retained austenite, cementite, undissolved graphite, and martensite. We have analyzed the amount of constituents present in the remelted layer by XRD analysis. Table 2 presents the results of microstructure

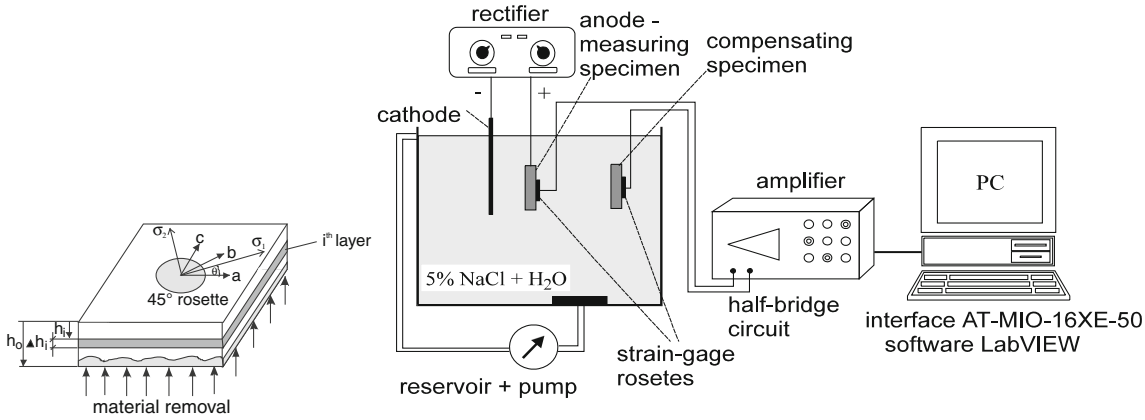

Fig. 5 Measuring system for residual stresses measurements by relaxation method with electro-chemical removal of modified surface layer

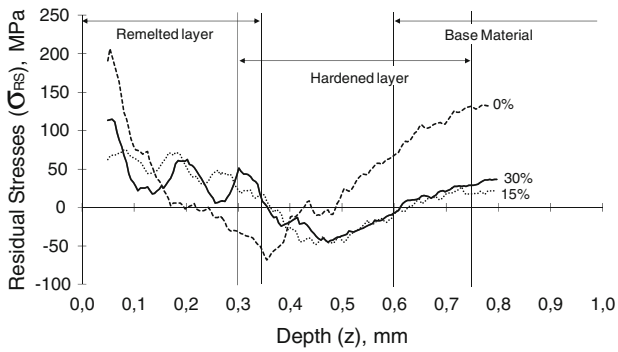

Fig. 6 Residual stresses in modified layer at different degrees of overlapping of the remelted traces, P = 1 kW, D_b = 3.3 mm, v_b = 21 mm/s, E = 14.4 J/mm^2

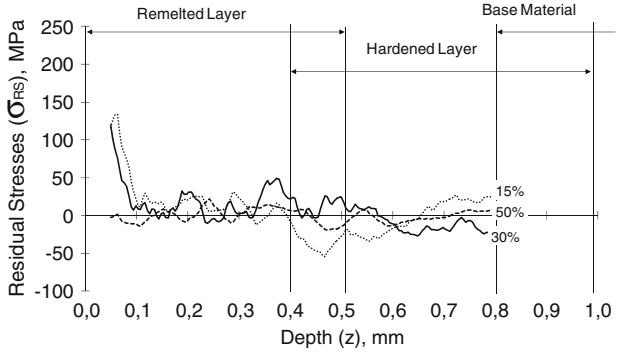

Fig. 7 Residual stresses in modified layer at different degrees of overlapping of the remelted traces, P = 1.5 kW, D_b = 5.1 mm, v_b = 18 mm/s, E = 16.3 J/mm^2

constituents measured at the surface of the remelted layer. In the remelted layer we can notice that by increasing energy input and overlapping degree, the amount of retained austenite decreases, and the amount of martensite increases.

The influence of laser energy input and laser beam overlapping degree on residual stresses at the surface of the remelted layer is shown in Table 3.

Figure 8 presents the correlation between residual stresses and the retained austenite measured at the surface of the remelted layer. The comparisons of residual stresses versus retained austenite were made for different laser heat treatment parameters (P, v_b, D_b, E_i). When vol.% of the retained austenite is increasing, tensile residual stresses are increasing too. The dependence could be described with linear function, as it is indicated in Fig. 8, where the correlation coefficient was between 0.8 and 0.87.

Table 3 Maximum tensile residual stresses σ_{RS} (MPa) at the surface of the remelted layer with respect to different laser process parameters

	Maximum residual stresses σ_{RS}, MPa	
Overlapping, %	E_i = 14.4 J/mm^2, D_b = 3.3 mm, P = 1 kW, d_b = 22 mm, v_b = 18 mm/s	E_i = 16.3 J/mm^2, D_b = 5.1 mm, P = 1.5 kW, d_b = 34 mm, v_b = 21 mm/s
0	220	150
15	180	130
30	120	100
50	40	0

Table 2 Constituents at the surface of the remelted layer in vol.%, analyzed by XRD

	Overlapping	Fe_γ, %	Fe_α, %	Fe_3C, %	Graphite	Min σ_{RS}, MPa	Max σ_{RS}, MPa
Figure 4; P = 1 kW, D_b = 3.3 mm,	0	22	41	32	5	150	220
E_i = 14.4 J/mm^2	30	10	49	37	4	50	120
Figure 5; P = 1.5 kW, D_b = 5.1 mm,	50	/	57	41	2	−30	0
E_i = 16.3 J/mm^2							

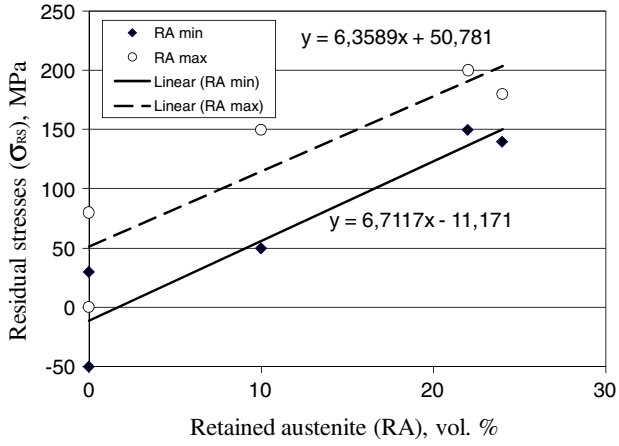

Fig. 8 Residual stresses (MPa) versus retained austenite (vol.%) measured at the surface of the remelted layer

The measured values of the residual stresses at the surface show that:

- Residual stresses at the remelted surface of nodular cast iron 500-7 almost always have a tensile character.
- The biggest residual stresses at the surface are obtained when there is no overlapping of the remelted traces.
- Higher degree of overlapping influences lower residual stresses. This is effecting by transformation of retained austenite into ferrite and cementite, and by tempering of martensite microstructure.

The overlapping degree of the remelted traces influences very much the temperature of the bulk specimen material, which also determines directly the cooling rates. High cooling rates have tendency to produce more retained austenite than martensite in the surface remelted layer. Temperatures obtained at the surface and at specific depths were calculated according to modified Ashby's equation (Eq 3) (Ref 22).

$$T(z,t) = T_0 + \frac{AP}{2\pi K v_b \sqrt{(t(t+t_0))}} e^{-\left(\frac{(z+z_0)^2}{4\alpha t}\right)} (^\circ\mathrm{C}) \qquad \text{(Eq 3)}$$

where T_0 (°C) is the initial temperature, A (/) is the absorptivity, P (W) is the laser beam power, K (W/mK) is the heat conductivity, v_b (mm/s) is the laser beam speed, t (s) is the time, $r_b = d_b/2$ (mm) is the laser beam radius, α (m^2/s) is the heat diffusivity, z (mm) is the coordinate.

Ashby has developed equation, which is suitable for description phase transformations in solid material. But in our case, we have also local surface melting. Because of that we have adopted this equation with a simple thermal model to get a good agreement between calculated thermal cycles and characteristic depths of modified layer. Thus, we have obtained a relatively simple mathematical model. This mathematical model describes the temperature evolution $T(z, t)$ in the material as a function of time and position. In the model, we have distinguished between the heating cycle and the cooling cycle (Eq 4, 5).

(1) *The Heating Cycle* conditions in the material can be described by the Eq 4:

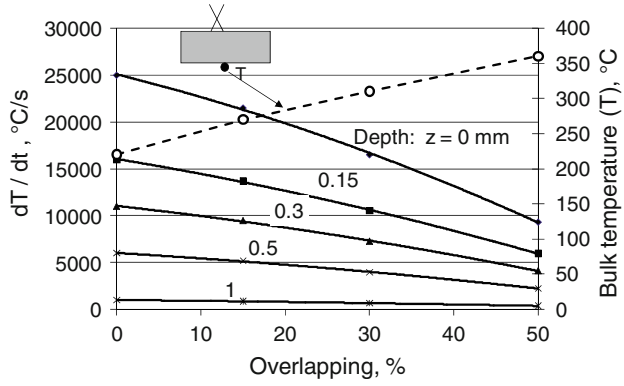

Fig. 9 Temperature rate dT/dt versus depth at different overlapping degrees of the remelted traces, P = 1.5 kW, d_b = 34 mm, v_b = 21 mm/s, E_i = 16.3 J/mm^2

$$T(z,t) = T_0 + \frac{AP}{2\pi K v_b \sqrt{t(t_i+t_0)}} \times \left[e^{-\left(\frac{(z+z_0)^2}{4\alpha t}\right)} + e^{-\left(\frac{(z-z_0)^2}{4\alpha t}\right)} \right] erfc\left(\frac{z+z_0}{\sqrt{4\alpha t}}\right) \qquad \text{(Eq 4)}$$

for $0 < t < t_i$

(2) *The Cooling Cycle* conditions in the material can be expressed by the Eq 5:

$$T(z,t) = T_0 + \frac{AP}{2\pi K v_b \sqrt{t(t_i+t_0)}} \times \left[e^{-\left(\frac{(z+z_0)^2}{4\alpha t}\right)} + e^{-\left(\frac{(z-z_0)^2}{4\alpha t}\right)} - e^{-\left(\frac{(z-z_0)^2}{4\alpha (t-t_i)}\right)} \right] erfc\left(\frac{z+z_0}{\sqrt{4\alpha t}}\right) \qquad \text{(Eq 5)}$$

for $t > t_i$where t_0 and z_0 are (Eq 6, 7):

$$t_0 = \frac{r_b^2}{4\alpha} \qquad \text{(Eq 6)}$$

$$z_0 = \sqrt{\frac{\pi \alpha r_b}{2eC v_b}} \qquad \text{(Eq 7)}$$

where t_0 (s) is the time necessary for heat to diffuse over a distance equal to the laser beam radius on the specimen surface, z_0 (mm) is the distance over which heat can diffuse during the laser beam interaction time t_i (s). C is a constant, in our case defined as C = 0.5.

The calculated temperature distribution in the surface modified layer was then the basis for the calculation of cooling rates dT/dt. The calculation is shown in Fig. 9. The temperature of the bulk material was measured at the bottom of the specimen during laser surface remelting process (secondary y-axis). In Fig. 9, we can see that maximum temperature at the bottom of the specimen increases from 220 to 360 °C when overlapping degree increases from 0 to 50%. This increase of bulk material temperature influences the decrease of cooling rates dT/dt, which is particularly important in the remelted surface layer (primary y-axis).

Lower cooling rates mean less retained austenite in the microstructure and consequently lower tensile residual stresses in laser remelted surface layer. In Fig. 9, we can see results of temperature measurements at the bottom of the specimen and calculations of cooling rates in the surface layer of the specimen for laser energy input of $E_i = 16.3$ J/mm^2 ($P = 1.5$ kW, $d_b = 34$ mm, $v_b = 21$ mm/s). We can notice the reduction of cooling rates with increasing the overlapping degree. The reduction of cooling rates is more distinct at the surface than at greater depths. Maximum temperatures of the bulk material are lower in the case of lower laser power $P = 1$ kW and lower energy input $E_i = 14.4$ J/mm^2. This consequently leads to higher cooling rates, and that means higher tensile residual stresses in the remelted material.

We have measured also the change in strain and temperature at the bottom of the specimen versus time during the laser surface remelting process in our previous research (Ref 16). The laser beam movement was resulting in a 0 and 30% overlapping of the remelted traces. In the case of a 0% overlapping of the remelted traces, a higher end specimen strain ($\varepsilon_a = 2.3$ μm/mm) is obtained than in the case of 30% overlapping ($\varepsilon_a = 2.1$ μm/mm). This is connected to the maximum temperature achieved in the specimen, which is higher in the case of 30% overlapping. Effects of preheating and tempering result in a lower specimen strain, and also in a lower residual stresses in the surface remelted layer.

Figure 10 presents calculated cooling rates and measured residual stresses at the remelted surface at different overlapping degrees of the remelted traces. One can find out that increasing the overlapping degree of the remelted traces influence on decreasing the cooling rates. Lower cooling rates decrease tensile residual stresses in the surface remelted layer. The effect of overlapping is clearly seen in decreasing the residual stresses. The dependence between the overlapping and the residual stresses is almost linear in the range from 0 to 30% of overlapping. But when we increase the rate of overlapping to 50%, the value of tensile residual stresses decreases much faster than the cooling rate. We can realize that preheating is increased. And an important role to residual stress reduction has tempering effect of the following remelted trace to the previous remelted trace. This tempering effect influences the reduction of retained austenite amount in the remelted layer and consequently the increase of martensite amount. When the optimum laser remelting parameters are achieved, i.e., lower cooling rates than 1.5×10^4 °C/s and high overlapping degree of remelted traces (higher than 40%), it is possible to obtain remelted surface of nodular cast iron 500-7 with almost no tensile residual stresses.

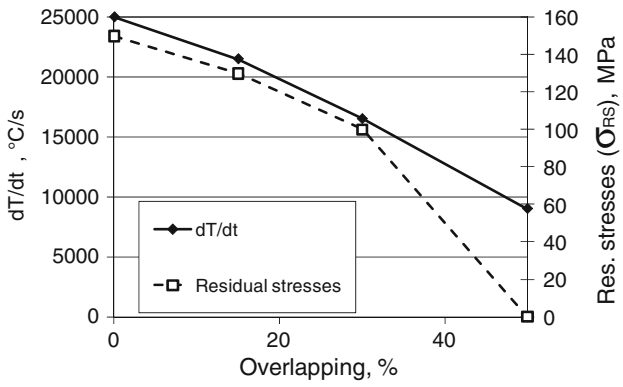

Fig. 10 Temperature rate and residual stresses at the remelted surface versus overlapping degree of the remelted traces, $P = 1.5$ kW, $d_b = 34$ mm, $v_b = 21$ mm/s, $E_i = 16.3$ J/mm^2

4. Summary

Laser surface remelting process induces tensile residual stresses in the remelted surface layer of nodular cast iron, which depend greatly on laser process parameters. High cooling rates cause phase transformations. In the remelted layer they cause local reduction of the microstructure volume, which could raise tensile residual stresses to even +200 MPa. On the other hand, in the hardened layer martensite transformation causes local increase of the microstructure volume and contributes to compressive residual stresses of maximum −80 MPa. From experiments it has been concluded that residual stress variation in the surface remelted layer is largely dependent on cooling rates. Lower cooling rates mean also lower residual stresses. We can achieve this with higher preheating by increasing energy input and overlapping degree. When cooling rates of the melt are less than 1.5×10^4 °C/s, considerably less retained austenite forms.

It is possible to achieve also a full release of tensile residual stresses at the surface of the remelted layer, but the overlapping degree must be higher than 40%. The main role for releasing tensile residual stresses in the remelted microstructure has tempering effect and transformation of retained austenite into ferrite and cementite ($\alpha + Fe_3C$). Thus at 50% overlapping of the remelted traces and at high enough laser energy input into the specimen surface ($E_i = 16.3$ J/mm^2, $P = 1.5$ kW, $D_b = 5.1$ mm, $d_b = 34$ mm, $v_b = 21$ mm/s), tensile residual stresses in the remelted layer were reduced to almost zero.

References

1. J. Michalski, J. Marszalek, and K. Kubiak, An Experimental Study of Diesel Engine Cam and Follower Wear with Particular Reference to the Properties of the Materials, *Wear*, 2000, **240**, p 168–179
2. G. Duffet, P. Sallamand, and A.B. Vannes, Improvement in Friction by cw Nd:YAG Laser Surface Treatment on Cast Iron Cylinder Bore, *Appl. Surf. Sci.*, 2003, **205**, p 289–296
3. J.H. Abboud, K.Y. Benyounis, A.G. Olabi, and M.S.J. Hashmi, Laser Surface Treatments of Iron-Based Substrates for Automotive Application, *J. Mater. Process. Technol.*, 2007, **182**, p 427–431
4. T. Slatter, H. Taylor, R. Lewis, and P. King, The Influence of Laser Hardening on Wear in the Valve and Valve Seat Contact, *Wear*, 2009, **267**, p 797–806
5. H. Sert, A. Can, H. Arikan, B. Selcuk, and H. Toprak, Wear Behavior of Different Surface Treated Cam Spindles, *Wear*, 2006, **260**, p 1013–1019
6. A. Roy and I. Manna, Laser Surface Engineering to Improve Wear Resistance of Austempered Ductile Iron, *Mater. Sci. Eng.*, 2001, **A297**, p 85–93
7. Y.P. Lei, H. Murakawa, Y.W. Shi, and X.Y. Li, Numerical Analysis of the Competitive Influence of Marangoni Flow and Evaporation on Heat Surface Temperature and Molten Pool Shape in Laser Surface Remelting, *Comput. Mater. Sci.*, 2001, **21**, p 276–290
8. A.P. Mackwood and R.C. Crafer, Thermal Modelling of Laser Welding and Related Processes: A Literature Review, *Opt. Laser Technol.*, 2005, **37**, p 99–115
9. K.Y. Benyounis, O.M.A. Fakron, J.H. Abboud, A.G. Olabi, and M.J.S. Hashmi, Surface Melting of Nodular Cast Iron by Nd:YAG Laser and TIG, *J. Mater. Technol.*, 2005, **170**, p 127–132

10. H.R. Shercliff and M.F. Ashby, The Prediction of Case Depth in Laser Transformation Hardening, *Metall. Trans. A*, 1991, **22A**, p 2459–2466
11. H. Pantsar, Relationship Between Processing Parameters, Alloy Atom Diffusion Distance and Surface Hardness in Laser Hardening of Tool Steel, *J. Mater. Process. Technol.*, 2007, **189**, p 435–440
12. H. Jiang and P. Woodard, Methodology of Generic Modeling as Applied to Energy Coupling CO_2 Laser Material Interaction, *Opt. Lasers Eng.*, 2005, **43**, p 19–31
13. K.M. Pedersen and N. Tiedje, Temperature Measurement During Solidification of Thin Wall Ductile Cast Iron. Part 1: Theory and Experiment, *Measurement*, 2008, **41**, p 551–560
14. Y. Chen, C.H. Gan, L.X. Wang, and A. Kaplan, Laser Surface Modified Ductile Iron by Pulsed Nd:YAG Laser Beam with Two-Dimensional Array Distribution, *Appl. Surf. Sci.*, 2005, **245**, p 316–321
15. K. Ahn, D. Kim, B.S. Kim, and C.H. Sohn, Numerical Investigation on the Heat Transfer Characteristics of a Liquid-Metal Pool Subjected to a Partial Solidification Process, *Progr. Nucl. Energy*, 2004, **44**(4), p 277–304
16. J. Grum and R. Šturm, Influence of Laser Beam Guiding and Overlapping on Residual Stress in Remelting Process, *Surf. Eng.*, 2005, **21**(1), p 27–34
17. A. Roy and I. Manna, Mathematical Modeling of Localized Melting Around Graphite Nodules During Laser Surface Hardening of Austempered Ductile Iron, *Opt. Lasers Eng.*, 2000, **34**, p 369–383
18. M. Tsujikawa, M. Hino, M. Kawamoto, and K. Okabayashi, Hard-Eye, Ductile Cast Iron And Its Treatment By Laser Quenching, *Proc. Int. Conf. on "Heat & Surface'92"*, Tokyo, Japan, 1992, p. 441–444
19. D.H. Jack and K.H. Jack, Carbides and Nitrides in Steel, *Mater. Sci. Eng.*, 1973, **11**, p 1–27
20. K.E. Thelning, Steel and its Heat treatment, 2nd ed., Bofors Handbook, Butterworth, London, UK, 1985
21. S. Hariri, R. Vaucher, P. Flahaut, D. Eyzop, and C. Robin, Residual stresses measurements by dissolution methods, *Proc. of the Int. Conf. "MAT-TEC' 96"*, Paris, France, 1996, p 111–118
22. M.F. Ashby and V.E. Easterling, The Transformation Hardening of Steel Surfaces by Laser Beams, *Acta Metall.*, 1984, **32**(11), p 1935–1984